Critical soliton speed for quantum reflection by a reflectionless potential well

U. Al Khawaja*

Physics Department, United Arab Emirates University, P.O. Box 15551, Al-Ain, United Arab Emirates

(Received 22 March 2021; revised 25 April 2021; accepted 17 May 2021; published 2 June 2021)

We consider the scattering of the nonlinear Schrödinger equation bright soliton by a reflectionless Pöschl-Teller potential well. We show that at the sharp transition between quantum reflection and full transmission, a single-node bound state localized at the center of the potential forms and is fully occupied. The profile and energy of the trapped mode are calculated both numerically and analytically using a variational calculation. The critical speed for quantum reflection is then determined from a delicate balance between the energy of the incident soliton and the energy of the trapped mode. We investigate the stability of the trapped mode against perturbations in its profile and position which explains the sharpness of the transition and sheds some light on the physics of quantum reflection. We show that quantum reflection by exciting the multinode trapped modes is also possible.

DOI: 10.1103/PhysRevE.103.062202

I. INTRODUCTION

Quantum reflection is an interesting phenomenon that reveals the wave nature of solitons when scattered by surfaces or steps [1–4], potential barriers [5–11], potential wells [11–15], or impurities [16–21]. It occurs at low soliton speeds and is understood by the formation of a trapped mode localized at the potential [15,19]. For solitons scattered by reflectionless potentials, quantum reflection occurs only below a critical speed where a sharp transition between full (quantum) reflection and full transmission takes place. Quantum reflection has been used to propose useful devices such as a soliton diode and logic gates [22–24]. Theoretically, a variational calculation that takes into account a trapped mode generates qualitatively the expected behavior [14,15]. However, an accurate calculation of the critical speed from a theoretical model is still missing. Our investigation shows that, unless an accurate profile and energy of the trapped mode are used, the critical speed can not be accounted for accurately.

Soliton scattering by a potential well shows sharp transition between full reflection and full transmission when the soliton internal energy is larger than the potential depth. The nonlinear interaction is in this case large enough to preserve the soliton integrity after scattering. If this condition is not met, then soliton splitting occurs and radiation is emitted. For reflectionless potentials [25], this condition is not required. The soliton integrity is always preserved and radiation is almost absent. This allows for the investigation of the phenomenon in terms of a wide range of potential depths. Here, we consider the scattering of bright solitons by the reflectionless Pöschl-Teller potential well. In the linear case, the spectrum of this potential is exactly accounted for in terms of bound states and their energies [26]. For the present nonlinear case, the spectrum is not known, to the best of our knowledge. Identifying the spectrum is essential to understand quantum reflection and resonant trapping since the trapped mode turns out to be the nonlinear single-node stationary state of the spectrum. Multinode states can also lead to quantum reflection but with wider potential widths, as will be detailed below.

Quantum reflection takes place when the energy of the incident soliton is less than that of the fully occupied trapped mode, while full transmission occurs in the opposite case. Therefore, the critical speed can be determined by equating the energy of the incident soliton with the energy of the trapped mode. This requires the knowledge of the profile and hence energy of the trapped mode. The calculation of critical speed for quantum reflection is challenging for two reasons. First, the critical speed corresponds to a trapped state located at a very sharp transition between full reflection and full transmission. This requires a high precision value of the trapped mode energy. Our first attempts with simplified variational calculations, showed that unless a particular form is used, the value of critical speed and its dependence on the potential depth will be either wrong or far from the accurate values and correct behavior. The second challenge arises from our quest to calculate the critical speed for a wide range of potential strengths ranging from weak to strong potentials compared to the internal energy of the soliton. It is particularly challenging to provide a unified theoretical account that describes both limits.

In the present paper, we revisit this problem with the aim of calculating the critical speed for a wide range of potential depths obtained from an accurate account of the profile and energy of the trapped mode. This is performed both numerically, using two independent approaches, and analytically using a variational method. While the three methods are independent, they share an excellent agreement on the critical speed, profile, and energy of the trapped mode. To understand why the transition between full reflection and full transmission is very sharp and to shed further light on the physics of quantum reflection, we investigate the stability of the trapped

*u.alkhawaja@uaeu.ac.ae

mode against perturbations in its profile and position. Finally, we present a procedure of obtaining the spectrum of the nonlinear multinode states of the Pöschl-Teller potential and verify that they also cause quantum reflection.

The rest of the paper is organized a follows. In the next section, we present our numerical approaches. In Sec. III, we present the variational calculation. In Sec. IV, we investigate the stability of the trapped mode. In Sec. V, we calculate some multinode trapped modes and verify quantum reflection for this case. In Sec. VI, we summarize and discuss our findings.

II. NUMERICAL CALCULATION

The scattering process is studied within the nonlinear Schrödinger equation (NLSE) in the presence of a potential,

$$i\frac{\partial}{\partial t}\psi(x,t)+\frac{1}{2}\frac{\partial^2}{\partial x^2}\psi(x,t)+g|\psi(x,t)|^2\psi(x,t) - V(x)\psi(x,t)=0, \tag{1}$$

where g is the strength of nonlinearity, which for the present case of bright soliton solutions should be positive. The Pöschl-Teller potential reads

$$V(x)=-V_0\,\mathrm{sech}^2(\alpha x), \tag{2}$$

where $\alpha=\sqrt{V_0}$ is a necessary condition for the soliton scattering by this potential to be reflectionless.

We start with the straightforward numerical approach, which we denote here and throughout as numerical-I, by tuning the soliton initial speed till the soliton is trapped by the potential for considerably long time. As an initial soliton, we use the exact movable bright soliton solution of the fundamental NLSE, namely, Eq. (1) with $V(x)=0$, which is given by [27]

$$\psi(x,t)=\frac{1}{2}\,n\sqrt{g}\,e^{i[vx+(\frac{1}{8}n^2g^2-\frac{1}{2}v^2)t]}\,\mathrm{sech}\Big[\frac{ng}{2}(x-vt)\Big], \tag{3}$$

where v is the soliton speed and n is an arbitrary positive constant that sets the central intensity and is equal to the norm of the soliton.

Our first numerical procedure for calculating the critical speed starts with solving numerically Eq. (1) with $\psi(x,0)$ as the initial profile. The critical speed is then found by a shooting method that varies the soliton initial speed such that both transmitted and reflected intensities vanish for a long evolution time. The critical speed can be computed with an increasing precision by sustaining the trapped state for longer times. The sharp transition between quantum reflection and transmission is shown in Fig. 1 where we plot reflectance, $R=(1/n)\int_{-x_f}^{-\Delta}|\psi(x,t_f)|^2dx$, and transmittance, $T=(1/n)\int_{\Delta}^{x_f}|\psi(x,t_f)|^2dx$. Here, $2x_f$ is the size of the spacial domain, t_f is an evolution time such that the scattered soliton is sufficiently far from the potential, and Δ is a length larger than the potential width. The norm is defined by

$$n=\int_{-x_f}^{x_f}|\psi(x,0)|^2dx, \tag{4}$$

which is calculated at $t=0$.

The second numerical procedure, which is denoted as numerical-II, is based on calculating the energy of the trapped

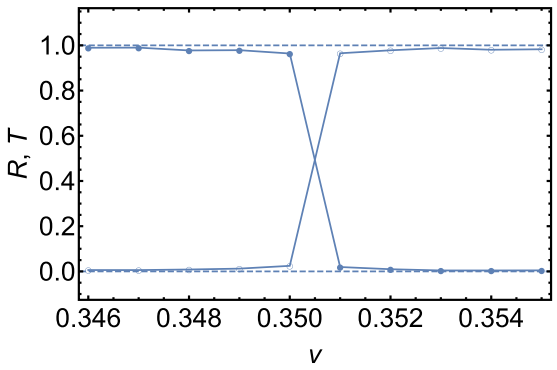

FIG. 1. Reflectance (filled circles) and transmittance (empty circles) versus initial soliton speed. Values of parameters used are: $V_0=2$, $g=1$, and $n=2$.

mode and equating it with the energy of the initial soliton. The energy of the initial soliton can be calculated from the energy functional corresponding to Eq. (1),

$$E_S=\int_{-\infty}^{\infty}\left[\frac{1}{2}|\psi_x(x,t)|^2-\frac{g}{2}|\psi(x,t)|^4\right]dx, \tag{5}$$

where ψ_x denotes partial derivative with respect to x. Since the soliton is initially far from the potential, the potential energy is vanishingly small and hence we do not include it in this energy functional. Using $\psi(x,0)$, given by Eq. (3), the energy of the initial soliton takes the form

$$E_S=\tfrac{1}{2}nv^2-\tfrac{1}{24}g^2n^3. \tag{6}$$

The energy of the trapped mode is, on the other hand, given by

$$E_T=\int_{-\infty}^{\infty}\left[\frac{1}{2}|\phi_x(x,t)|^2-\frac{g}{2}|\phi(x,t)|^4+V(x)|\phi(x,t)|^2\right]dx, \tag{7}$$

where $\phi(x,t)$ is the trapped mode solution of Eq. (1).

Equating the energy of the soliton to that of the trapped mode, the critical speed will be given by

$$v_c=\sqrt{\frac{1}{12}g^2n^2+\frac{2}{n}E_T}. \tag{8}$$

Hence, it is essential to calculate the energy of the trapped mode to calculate the critical speed.

Examining the profile of the trapped mode, we notice that it is always composed of two peaks separated by a node at the center of the potential with a linear dependence $\phi(x,t)=\delta(t)\,x$, around $x=0$, where $\delta(t)$ reaches its maximum when the mode is fully occupied. We thus conjecture that the trapped mode is a stationary solution of the NLSE, Eq. (1), that is localized at the potential and has a node at the center. Substituting the general form of stationary solution $\psi(x,t)=\phi(x)\,\exp(-i\mu t)$ in Eq. (1) gives

$$\mu\phi(x)+\frac{1}{2}\frac{\partial^2}{\partial x^2}\phi(x)+g\phi^3(x)-V(x)\phi(x)=0, \tag{9}$$

where the soliton frequency, μ (or chemical potential in the case of matter-wave solitons of Bose-Einstein condensates),

is related to the trapped mode energy by

$$E_T = n\mu + \frac{g}{2}\int_{-\infty}^{\infty} \phi^4(x)dx, \tag{10}$$

which can be obtained by multiplying Eq. (9) by $\phi(x)$, integrating over all space, and then comparing with Eq. (7). Stationary trapped modes and their energies are obtained by solving Eq. (9). Based on the above-mentioned general structure of the trapped mode, the boundary conditions needed to calculate the trapped mode are $\phi(0) = 0$ and $\phi_x(0) = \delta$, where we have removed the time dependence since we are looking for a stationary solution. Two more restrictions need to be taken into account while solving this equation. First, the trapped mode has to decay outside the potential to zero, and second, the norm of the trapped mode has to be equal to that of the initial soliton. The numerical procedure is therefore implemented in two steps. First, we solve numerically Eq. (9) with the above-mentioned boundary conditions using trial values of central slope, δ, and soliton frequency, μ. This results typically in an oscillatory solution. Then we search for the value of μ that pushes the oscillations away from the localization. With adequate fine-tuning of μ, a localized nonoscillatory solution will be obtained. The second step is to calculate the norm of the resulting state and require that it equals the norm of the initial soliton, n. To achieve this criterion, the value of δ is now varied and the search procedure for localized solution using μ is repeated. Ultimately, a localized stationary solution that corresponds to the profile and energy of the trapped mode as well as the norm of the initial soliton will be obtained.

Computing the trapped mode frequency, μ, and its central slope, δ, with arbitrary accuracy using the above-described numerical procedure turns out to be computationally demanding, which is described as follows. We use a typical ordinary differential equation solver such as the Runge-Kutta fourth order (RK4) to solve Eq. (9). For higher accuracy, the iterative power series method may be used [28]. For quick convergence, we use the variational values of μ and δ, which are calculated in the next section, as starting values for the search procedure. Alternatively, one may find such 'good' starting values by inspection. Most likely, the solution with these starting values will not be the sought localized solution and it will be rather an oscillatory solution. The task is then to vary μ, such that a non oscillatory localized solution with a decaying tail is obtained. The question is then how to set such a criterion numerically? One may attempt to set the condition that the solution vanishes at the end of the spacial domain, x_f. This does not lead to an accurate solution since the exact value of the solution at x_f, while very small, is not zero. In addition, an oscillatory solution may have one of its nodes at x_f and thus satisfying the condition while it is not the targeted localized solution. Based on the observation that the localized mode must have the lowest norm among all oscillatory solutions, we calculate the norm for a range of μ values including its critical value. The critical value will then be distinguished by a sharp dip in the curve as shown in Fig. 2. The middle subfigure shows a zoom near the bottom of the dip of the upper subfigure where another much narrower dip appears again. The bottom subfigure shows again a zoom of the bottom of the dip in the middle subfigure. A third dip does not appear since, for the $x_f = 20$ which we consider, the solution is localized. Had we used a larger x_f, a third dip would appear. This successive appearance of minima reflects the refinements in the value of μ as we approach the critical value, as shown in Fig. 3. In principle, one can determine the critical value of μ using this procedure to an arbitrary accuracy. However, as we mentioned above, the accuracy of the differential equation solver sets a limit on the maximum accuracy of the critical μ obtained by this procedure. This will be evident by making further zooms in the curve which will end up with a noisy curve signifying reaching the scale of the errors in the differential equation solver. Another important factor to pay attention to is x_f. The computed critical values obtained with this procedure will be closer to the exact value for larger x_f. This will, however, require more computational

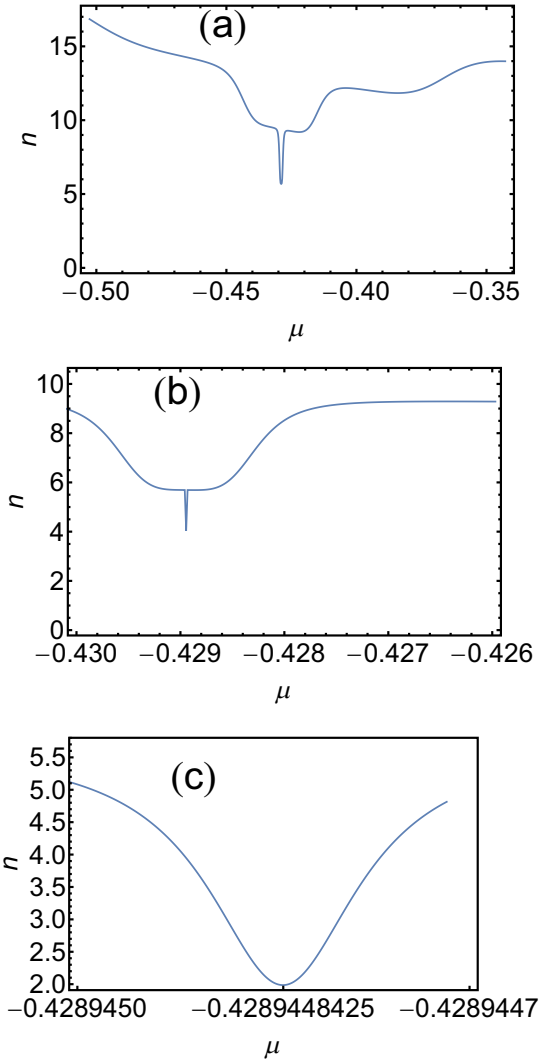

FIG. 2. Norm, as defined by Eq. (4), in terms of the trapped soliton frequency μ. Subfigure (b) is a zoom to the bottom of the dip in subfigure (a). Subfigure (c) is a zoom to the minimum of the dip in subfigure (b). The values of μ at the minima, starting from the upper sub figure, correspond to refinements of the computed value. The search for localized state started with $\mu = -0.25$ and $\delta = 7.3$. The values of other parameters used are: $V_0 = 62$, $x_f = 20$, $g = 1$, $n = 2$.

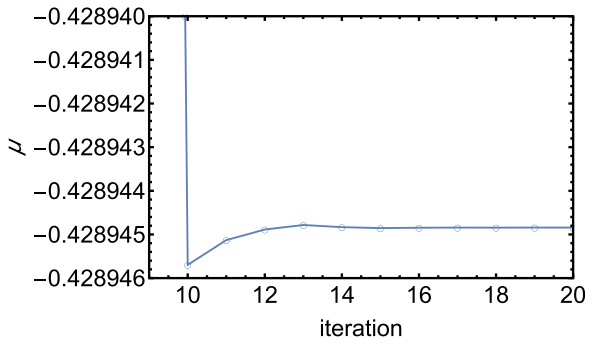

FIG. 3. Computed values of the trapped soliton frequency μ in terms of the refinement iteration. The figure corresponds to the specific case of Fig. 2. Starting from the trial value of $\mu = -0.25$, the curve saturates at $\mu = -0.4289448427098$.

time. Numerically, it is challenging to search for such sharp minima embedded in a much wider range. To be able to detect the minimum at the dip, a step size of the order of or smaller than the width of the dip is to be used. If we use this very small step size to search for the dip in the much wider background, then the calculation will be excessively time consuming. We solve this problem as follows. First, we find μ at the minimum of the first dip using a rather large step size in μ. Then, to find the minimum of the second dip, we reduce the step size by a factor that depends on the magnitude of the difference between the starting value of μ and the one found at the first dip. This procedure is repeated for the next iterations such that for each dip the step size of the search method is reduced to a suitable value for the scale at which the dip occurs. In this manner, the critical values will be computed with arbitrary accuracy up to the differential equation solver accuracy. While we have only explained the procedure of computing μ, a similar procedure is followed for finding the slope δ.

The result of the above two numerical procedures are shown in Fig. 4 where we plot the critical speed versus a

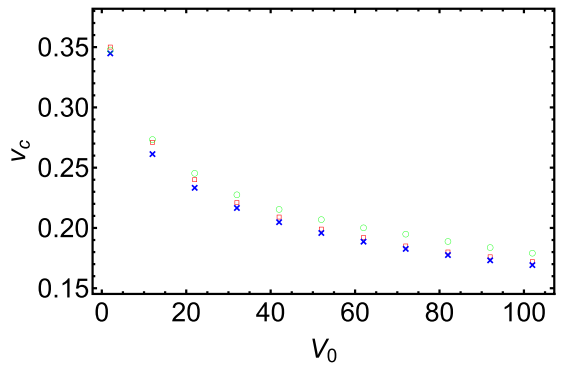

FIG. 4. Critical soliton speed, v_c, at which the soliton will be trapped by the potential in terms of its depth, V_0. Crosses correspond to the numerical calculation of the energy of the trapped mode (numerical-I). Squares correspond to the numerical calculation of the initial soliton energy that leads to trapping (numerical-II). Circles correspond to the variational calculation. Values of parameters used are: $g = 1$ and $n = 2$.

TABLE I. Trapped mode energy of the Pöschl-Teller potential Eq. (2) in terms of its depth, V_0, calculated using three independent methods. Numerical-I method is to calculate the energy using the stationary localized numerical solution of NLSE Eq. (9). Numerical-II is to calculate the initial soliton energy such that its scattering with the potential leads to a trapped mode. Variational calculation uses the trial solution Eq. (11) to calculate the energy functional Eq. (7).

	E_T		
V_0	Numerical-I	Numerical-II	Variational
2	−0.303509	−0.304217	−0.301112
12	−0.302110	−0.302857	−0.299411
22	−0.300678	−0.301305	−0.297529
32	−0.298844	−0.299452	−0.295196
42	−0.296192	−0.297212	−0.293117
52	−0.293442	−0.294420	−0.290343
62	−0.289344	−0.290803	−0.286755
72	−0.284162	−0.285808	−0.281378
82	−0.275369	−0.278242	−0.272931
92	−0.259473	−0.264321	−0.258392
102	−0.210277	−0.213457	−0.212189

wide range of potential depths. Both methods lead to almost identical values. In addition, we list in Tables I and II lists of numerical values of the trapped mode energy and critical soliton speed calculated using these two numerical methods and the variational method which we describe in the next section. An example of a stationary state corresponding to the trapped mode for $V_0 = 2$ and $V_0 = 102$ are shown in Fig. 5. An important difference between the two procedures need to be pointed out. In the first numerical procedure, where an incoming soliton, is trapped by the potential, there will be always some left over kinetic energy that results in internal oscillations of the trapped mode. Thus the profile of the trapped mode will be oscillating around the exact one which we consider as the one generated by the second procedure. This slight mismatch is clear in the figure.

For verification of the above results and further insight, we perform a variational calculation in the next section.

TABLE II. Critical speed for soliton trapping calculated using three independent methods as described in Table I.

	v_c		
V_0	Numerical-I	Numerical-II	Variational
2	0.351	0.346231	0.348058
12	0.272	0.262702	0.273755
22	0.241	0.234716	0.245768
32	0.222	0.218002	0.227936
42	0.210	0.206228	0.215820
52	0.200	0.197265	0.207340
62	0.193	0.190055	0.200539
72	0.186	0.184070	0.195288
82	0.181	0.178963	0.189221
92	0.177	0.174576	0.184181
102	0.173	0.170634	0.179504

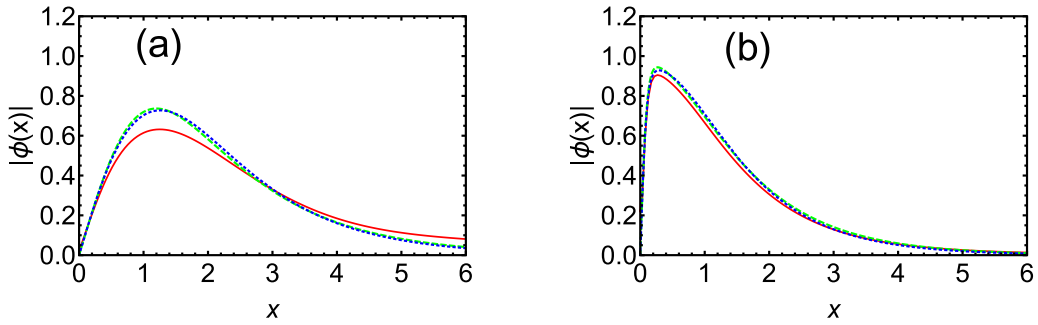

FIG. 5. Profile of the single-node trapped mode. Dotted (blue) curve corresponds to the numerical solution of Eq. (9) with $\mu = -0.2198$ and $\phi'(0) = 1.09$ for $V_0 = 2$ (a) and $\mu = -0.4419$ and $\phi'(0) = 9.8$ for $V_0 = 102$ (b). Solid (red) curve corresponds to the trapped mode resulting from the scattering of a soliton at the critical speed. Dashed (green) curve corresponds to the variational calculation. Values of other parameters used are: $g = 1$ and $n = 2$.

III. VARIATIONAL METHOD

Due to the sharpness of transition in scattering behavior at the critical point, it is not easy to account for the numerical results with a theoretical model unless an exact or very accurate profile of the trapped mode is used. To the best of our knowledge, the spectrum of the nonlinear stationary states of the Pöschl-Teller potential are not known, unlike its linear counter part. Nonetheless, we provide here a variational calculation that proposes a profile of the trapped mode that leads to the numerical results of the previous section to a high degree of accuracy.

Initially, we have used many trial functions that account for the node and general structure of the trapped mode. For instance, we have used the simple trial functions $x\,\mathrm{sech}(cx)$, $x\,\exp(-c|x|)$, $(c_1x + c_2x^3)\mathrm{sech}(c_3x)$, $x\,\exp(-cx^2)$, etc., but all of these trial functions did not lead to even a qualitative agreement with the numerical results. In Ref. [29], nodal and nodeless families of solutions to the U(1)-Higgs model where found using a multiscale expansion. While the model considered by that reference is slightly different than ours, the method may be modified to obtain an approximate single node solution which may serve as a trial function to the present variational calculation. The proper trial function is inspired, in fact, by the linear case where a linear Schrödinger equation with a Pöschl-Teller potential can be transformed to the Legendre equation in terms of the variable $u = \tanh(x)$. The first Legendre polynomial with a node is $\tanh(x)$. Since in the present nonlinear case, the trapped mode needs also to be localized, we propose the following trial function:

$$\phi(x) = A\,\mathrm{sech}(\gamma x)\tanh(\beta x), \tag{11}$$

where A is a normalizing constant, γ and β are variational parameters. The parameter β accounts to the central slope while the parameter γ accounts to the overall width of the mode. First, we normalize the trial function to n, which results in

$$A[\gamma,\beta] = \frac{\sqrt{n}}{\int_{-\infty}^{\infty}\mathrm{sech}^2(\gamma x)\,\tanh^2(\beta x)dx}. \tag{12}$$

The integration can not be obtained in a closed analytical form. One of the parameters can be scaled out and the resulting one-parameter integral can be fit with an approximate function. However, we did not find a simple fit that leads to the correct numerical results. Therefore, we leave this integral and similar ones in the energy functional to be calculated numerically in terms of γ and β. Substituting the normalized trial function in the energy functional Eq. (7), we get

$$E_T[\gamma,\beta] = A^2[\gamma,\beta]\left\{\frac{1}{2}\int_{-\infty}^{\infty}\mathrm{sech}^2(\gamma x)[\beta\,\mathrm{sech}^2(\beta x) - \gamma\tanh(\beta x)\tanh(\gamma x)]^2dx - \frac{gA^2[\gamma,\beta]}{2}\int_{-\infty}^{\infty}[\mathrm{sech}(\gamma x)\tanh(\beta x)]^4dx - V_0\int_{-\infty}^{\infty}\mathrm{sech}^2(\alpha x)[\mathrm{sech}(\gamma x)\tanh(\beta x)]^2dx\right\}. \tag{13}$$

Plotting $E_T[\gamma,\beta]$ for specific values of n, g, and V_0, shows that it indeed has a local minimum at specific values of $\gamma = \gamma^*$ and $\beta = \beta^*$. Substituting back these specific values in the energy functional, we obtain the minimum energy, $E_T[\gamma^*,\beta^*]$, which is supposed to correspond to the energy of the trapped mode. Inserting this energy value in Eq. (8), gives the critical speed.

Figure 4 and Tables I and II show good agreement between the variational calculation and the numerical results for the critical speed and trapped mode energy. In addition, the profile of the trapped mode is almost indistinguishable from the numerical one indicating that our trial function, not only produces the correct energy of the trapped mode, but also describes accurately its profile. In Fig. 6, we plot the variational trapped mode energy and the variational parameters γ^* and β^* versus the potential depth, V_0. The energy of the initial soliton shown by the dotted line in the subfigure for trapped mode energy is always less than that of the trapped mode. The difference between the two energies is the initial translational kinetic energy needed for the soliton to be trapped. To a good approximation, the parameter β^* behaves as $\sqrt{V_0}$.

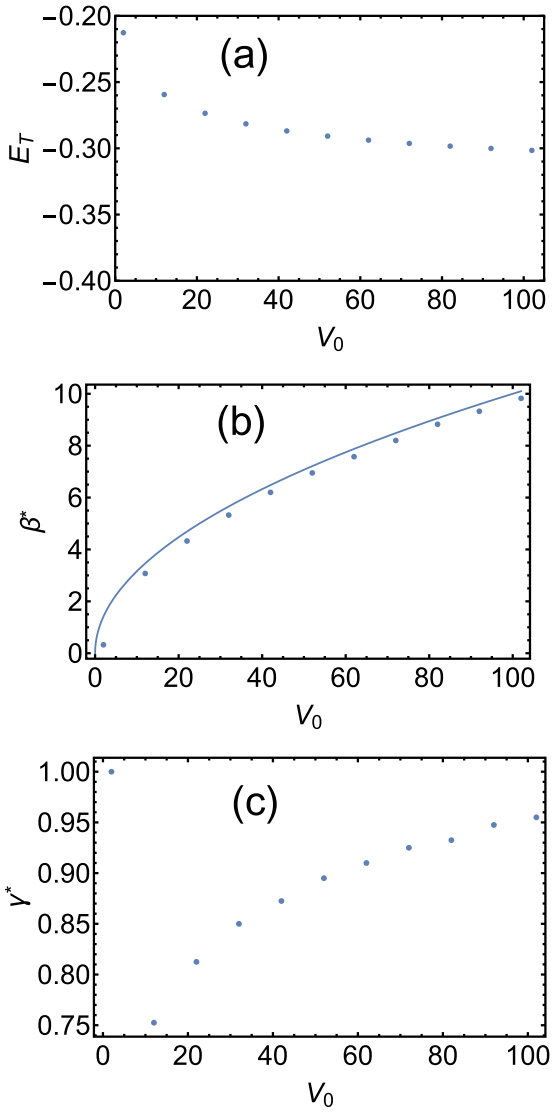

FIG. 6. Trapped mode variational energy, E_T, and variational parameters γ^* and β^* at the minimum of $E_T[\gamma, \beta]$. Dotted horizontal line in subfigure (a) corresponds to the energy of a stationary initial soliton. The curve in subfigure (b) is $\sqrt{V_0}$. Values of parameters used are: $g = 1$ and $n = 2$.

The linear expansion of the trial function Eq. (11) around $x = 0$, the central slope will be given by $\delta \approx A\,\beta$, which is approximately equal to β since A is close to 1 for the whole range of V_0 considered. However, and due to the sensitivity of the calculation at the critical speed, this seemingly good approximation is not enough to account for the numerical values.

It is instructive to model the scattering of the soliton by the motion of a classical object. To that end, we calculate the effective potential experienced by the soliton during scattering. A time-dependent variational calculation gives the equation of motion for the position of the soliton peak, $x_0(t)$, from which the effective potential is extracted. Using the movable form of a localized solution $\psi(x,t) = \phi[x - x_0(t)] \exp iv(t)[x - x_0(t)]$, where $\phi(x)$ takes the form of Eq. (11), the Lagrangian corresponding to Eq. (1),

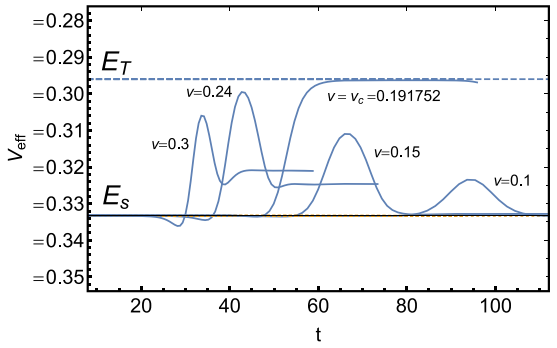

FIG. 7. Effective potential for a soliton scattered by the Pöschl-Teller potential with speeds less than, equal to, and larger than the critical speed. The horizontal dashed and dotted lines correspond to the energy of the single-node trapped mode energy, E_T, and the stationary initial soliton energy, E_s, respectively. Values of parameters used are: $g = 1$, $V_0 = 62$, $n = 2$. Initial soliton position is $x_0(0) = -10$ and time of evolution equals $1.8 \times |x_0(0)|/v$.

namely, $L = \int_{-\infty}^{\infty}[(i/2)(\psi_t\psi^* - \psi^*\psi_t) - (\frac{1}{2}|\psi_x|^2 - \frac{g}{2}|\psi|^4 + V|\psi|^2)]dx$, leads to the equation of motion

$$n\ddot{x}_0(t) = -\frac{d}{dx}V_{\text{eff}}[x_0(t)], \tag{14}$$

where

$$V_{\text{eff}}[x_0(t)] = \int_{-\infty}^{\infty}\left\{\frac{1}{2}\left[\frac{d}{dx}\phi(x)\exp(ivx)\right]^2 - \frac{g}{2}\phi^4(x) + V(x)\phi^2[x - x_0(t)]\right\}dx \tag{15}$$

is the effective potential. It is only the potential term that introduces the x_0-dependence to the effective potential. In Figs. 7 and 8, we plot the effective potential for soliton speeds less than, equal to, and greater than the critical speed versus time and soliton peak position, respectively. For $v < v_c$, Fig. 8 shows that the dynamics is similar to an object of initial kinetic energy launched from the left, then rising up the potential ramp till it reaches a maximum height with vanishing speed. The object will then fall back which accounts for the quantum reflection of the soliton. At the critical speed, $v = v_c$, the maximum height of the potential ramp matches exactly the energy of the single-node trapped mode. For $v > v_c$, the potential takes the shape of a potential barrier continued in the positive x range. The initial kinetic energy in this case is larger than the maximum height of the barrier and therefore, it will cross it with a nonzero speed. This corresponds to the full transmission case. In terms of time, the potential at the critical speed takes the form of a potential step, as shown by Fig. 8. The object has an initial kinetic energy barely enough to reach the plateau with zero speed and remains there indefinitely. This corresponds to the critical state of the soliton being fully trapped by the potential.

IV. STABILITY OF TRAPPED MODES

To gain further insight into the physics of quantum reflection and explain why the transition between full reflection and full transmission at the critical speed is very sharp, we

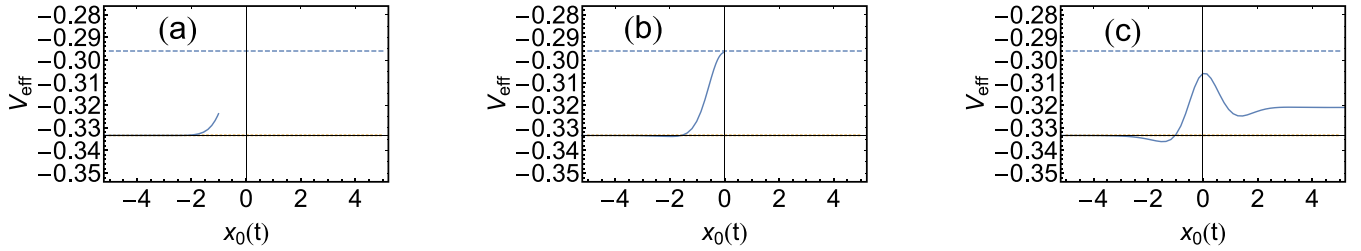

FIG. 8. Three curves from Fig. 7 replotted versus the position of the soliton peak, $x_0(t)$. Soliton initial speeds equal $v = 0.1$ for (a), $v = v_c = 0.191752$ for (b), and $v = 0.3$ for (c).

investigate the stability of the trapped mode. The variational calculation shows that the trapped mode corresponds to a minimum of the energy functional in terms of the width of the mode and slope of its node given by $1/\gamma$ and β, respectively. In Fig. 9, we show this for $V_0 = 12$. While the trapped mode is stable against small perturbations in these parameters, we found that it is very unstable against variations in its position. If the trapped mode is shifted slightly from its equilibrium position, then it gets ejected out of the potential as a soliton. This is shown in Fig. 10 where a trapped mode was shifted, initially by $\pm 10^{-5}$, has been ejected to the left or right of the potential and remarkably emerges as a soliton with the critical speed for trapping. This can be verified theoretically by considering a shifted trapped mode $\phi(x - x_0)$ to expand the energy functional Eq. (7) around $x_0 = 0$ as follows:

$$E_T[x_0] = E_T + \left[\frac{1}{2}\frac{\partial^2}{\partial x_0^2}\int_{-\infty}^{\infty} V(x)\phi^2(x - x_0)dx\right]_{x_0=0} x_0^2, \tag{16}$$

where the zeroth-order term is the trapped mode energy, the first-order term vanishes because the integrand is an odd function, and only the potential integration contributes to the second order term since in the other terms a shift of coordinates removes x_0. For the trial function Eq. (11), the last expression becomes

$$E_T[x_0] = E_T - V_0\left\{\int_{-\infty}^{\infty}[\cosh(2\sqrt{V_0}\,x) - 2]\text{sech}^4(\sqrt{V_0}\,x)\tanh^2(\beta x)\text{sech}^2(\gamma x)dx\right\} x_0^2. \tag{17}$$

Inspection shows that the integral in the square brackets is always positive for the range of parameters used, namely, $V_0 \in [2, 102]$. Therefore, we conclude that $E \propto -x_0^2$, i.e., the trapped mode corresponds to an energy maximum in terms of x_0. For the particular case of $V_0 = 12$ and its variational parameters $\gamma^* = 0.74$ and $\beta^* = 3.01$, we calculate the energy functional using the trial function Eq. (11) and compare it with the above expression which in this case takes the form $E_T \approx -0.26 - 17.7x_0^2$. In Fig. 11, both results agree for small x_0 and show that the energy functional has indeed a maximum, rather than a minimum at $x_0 = 0$. This explains the unstable dynamics described above.

Based on all of the above, we can now synthesise a description to the dynamics of quantum reflection and critical behavior as follows. The incoming soliton starts to populate the trapped mode mainly from its translational kinetic energy. If the latter is not sufficient to fully populate the trapped mode, then the soliton will stop moving before the trapped mode reaching a profile that has the same norm as the initial soliton and thus will be an imbalanced profile—the intensity towards the incoming soliton side is larger than that on the other side—such that it corresponds to an effectively shifted profile towards the direction of the incoming soliton. According to the above stability analysis, the trapped mode will be ejected towards the same direction, and this corresponds to quantum reflection. On the other hand, if the kinetic energy of the soliton is large enough such that the trapped mode will be fully populated and then imbalanced towards the opposite direction of the incoming soliton, the trapped mode will be ejected from that direction as a soliton and this corresponds to transmission. At the critical speed, the kinetic energy is exactly sufficient to populate the trapped mode such that its norm is equal to that

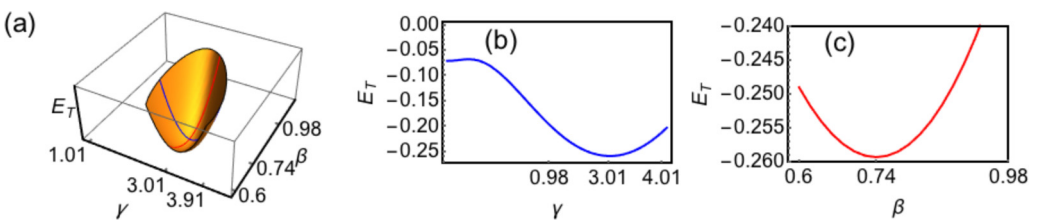

FIG. 9. Minimum of variational energy of single-node trapped mode in terms of its variational parameters. Values of parameters used are: $g = 1$, $V_0 = 12$, $n = 2$. Subfigures (b) and (c) are cross sections of the surface plot in subfigure (c).

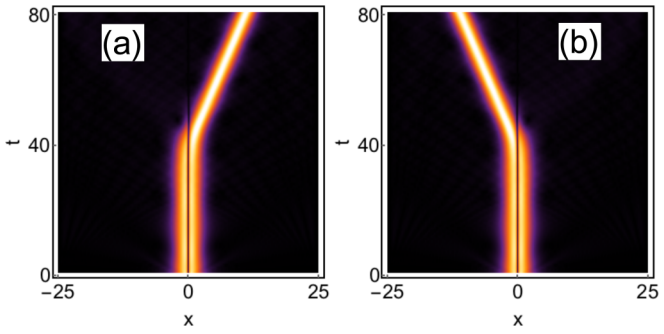

FIG. 10. Trapped single-node mode ejected as a soliton due to an infinitesimal shift of 10^{-5} for subfigure (a) and -10^{-5} for subfigure (b). Ejected soliton speed equals the critical speed for soliton trapping. Values of parameters used are: $g = 1$, $V_0 = 12$, $n = 2$.

of the incoming soliton and this corresponds to a balanced trapped mode. At the same time, the kinetic energy of the initial soliton has vanished and no more pumping of energy is available.

V. MULTINODE TRAPPED MODES

Here we calculate the first few of the nonlinear multinode stationary states of the Pöschl-Teller potential and verify that they also lead to quantum reflection. While we will use here the second numerical procedure described in Sec. II, we remark first about how the multinode solutions may be obtained variationaly. Similar to the argument led to the single-node solution, multinode trial solutions would contain the higher order Legendre polynomials in $\tanh(\beta x)$, namely, $\phi(x) = \mathrm{sech}(\gamma x)\,\tanh^{2k+1}(\beta x)$, where k is a positive integer.

Following the second numerical procedure of Sec. II, it turns out that it is not possible to find a multinode non oscillatory stationary state if the inverse width of the potential is related to its amplitude strictly by $\alpha = \sqrt{V_0}$, i.e., when the Pöschl-Teller potential is a reflectionless potential. Therefore, we investigated the possibility of relaxing the reflectionless condition by setting potential widths wide enough to accommodate multinode solutions. Naturally, for larger number of

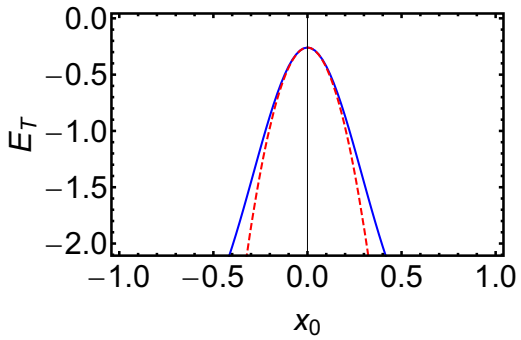

FIG. 11. Energy of trapped single-node mode in terms of displacement with respect to the center of the potential. Solid (blue) corresponds to the variational calculation and dashed (red) corresponds to the expansion Eq. (17). Values of parameters used are: $g = 1$, $V_0 = 12$, $n = 2$.

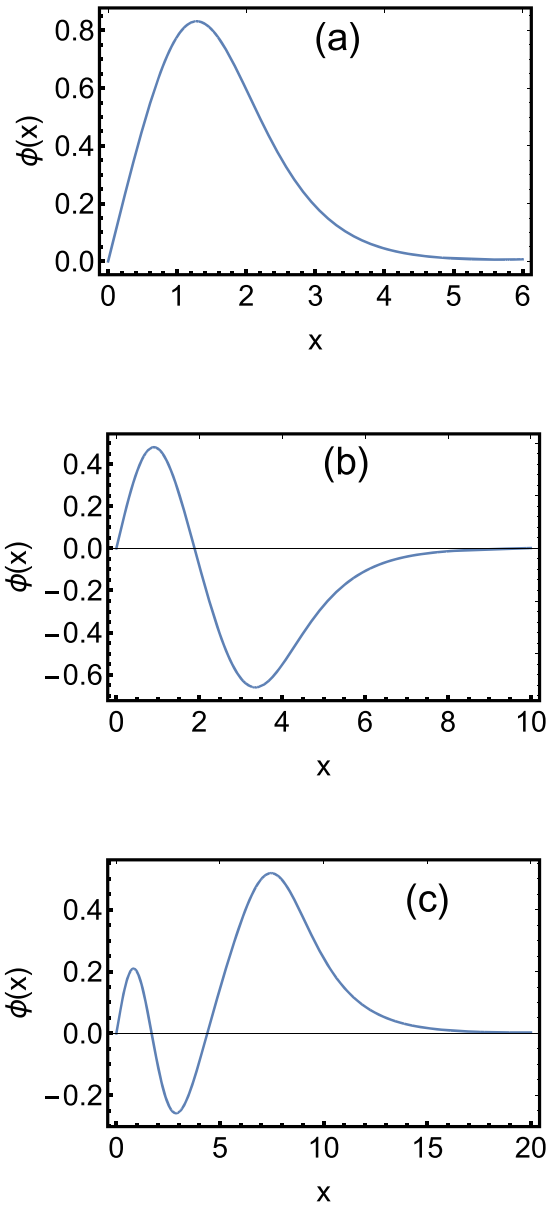

FIG. 12. Nonlinear trapped mode stationary states and energies of the potential $V(x) = -V_0\mathrm{sech}^2(\sqrt{V_0}x/4)$ for $V_0 = 2$. Values of initial slope are 0.96, 0.83, and 0.40 for the single (a), triple (b), and quintic (c) nodes solution, respectively. Values of parameters used are: $g = 1$ and $n = 2$.

nodes, wider potential width is needed. In Fig. 12, we plot the profile of the first few multinode solutions for specific values of normalization, nonlinearity strength, and potential depth.

Quantum reflection by a multinode trapped mode is shown in Fig. 13 for the potential $V(x) = 62\,\mathrm{sech}^2(\sqrt{62}\,x/3)$ and norm $n = 4$. The figure shows clearly the formation of a three-node trapped mode. Solving independently the NLSE with this potential and norm using the numerical method described in Sec. II, the exact stationary three-node solution is obtained. Both profiles are shown also in Fig. 13 with an agreement on the number and location of the nodes. The maxima in the profile obtained by the scattering experiment are less than those of the exact solution because the trapped mode is not

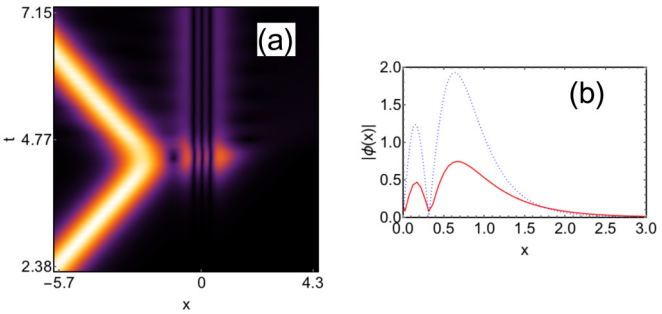

FIG. 13. (a) Quantum scattering of soliton by the three-node trapped mode of the potential $V(x) = -V_0\,\mathrm{sech}^2(\sqrt{V_0}x/4)$ for $V_0 = 62$. (b) Profile of the maximally occupied trapped mode. Dotted (blue) curve is the result of the numerical solution of Eq. (9) and solid (red) curve is the maximally occupied trapped mode obtained by the scattering shown in the left subfigure. Values of parameters used are: $g = 1$ and $n = 4$.

fully trapped. One can also show that when the speed is large enough, the soliton will pass through the potential leaving a small three-node trapped mode behind. Due to the fact that the potential we use here is not purely reflectionless, the sharp transition between full reflection and full transmission is not present. Instead, there will be a range of soliton speeds where a considerable portion of the soliton is trapped. For the case of Fig. 13, almost full quantum reflection occurs for speeds less than about 0.8. For speeds larger than 1.5, the soliton will transmit but with a residual small three-node mode left trapped. Between these two speeds, the scattered soliton is split between trapped part, transmitted part, and a considerable amount of radiation.

VI. DISCUSSION AND CONCLUSIONS

We have calculated the critical speed for quantum reflection of a bright soliton scattered by the reflectionless Pöschl-Teller potential in terms of its depth. The calculation was performed both numerically and variationaly with very good agreement on critical speed and trapped mode energy and profile. Quantum reflection and resonant trapping were explained in terms of the single-node stationary mode of the potential. The accurate account of profile and energy of the trapped mode was essential to calculate the critical speed. Using the variational calculation, we mapped the dynamics of the soliton to a classical object launched up a potential ramp in the case of quantum reflection, a potential barrier in the case of full transmission, and a potential step in the case of resonant trapping. To understand the reason for the sharp transition between full reflection and full transmission, we have investigated the stability of the trapped mode against perturbations in its width and position. It turned out that, while the trapped mode is stable against perturbations in its width, it is very unstable against perturbation in its equilibrium position. Consequently, the time-reversal of soliton trapping was generated, namely, an initially trapped mode is ejected as a bright soliton moving with the critical speed. We have also verified that quantum reflection may occur by exciting the multinode trapped modes and found the profile and energy of the first few of them.

The original aim of this work was to obtain an analytical formula for the critical speed in terms of the potential depth in a generalization to the linear case. However, the integrations needed to be performed using the trial solution Eq. (11) and energy functional of the trapped mode Eq. (7), such as $\int_{-\infty}^{\infty} \mathrm{sech}^2(\gamma x)\,\tanh^2(\beta x)dx$, turned out to be not integrable in analytical form. We have used alternative interpolations, but as we mentioned earlier, the high degree of accuracy required at the critical speed, required more accurate calculation of the energy of the trapped mode.

We were unable to find a rigorous proof for that only the single-node trapped mode being excited when the potential well is reflectionless. This needs to be investigated further also for other potentials. We had to break the reflectionless condition $\alpha = \sqrt{V_0}$ to excite the multinode trapped modes; we needed to have a wider potential such that more nodes can be accommodated. However, this poses the question of whether multinode trapped modes do exist or do not for the reflections Pöschl-Teller potential.

ACKNOWLEDGMENT

The author acknowledges the support of UAE University through Grants No. UAEU-UPAR1 and No. UAEU-UPAR11.

[1] F. Baronio, C. De Angelis, P. Pioger, V. Couderc, and A. Barthélémy, Opt. Lett. **29**, 986 (2004).
[2] H. Friedrich and J. Trost, Phys. Rep. **397**, 359 (2004).
[3] R. Cote, H. Friedrich, and J. Trost, Phys. Rev. A **56**, 1781 (1997).
[4] M. Lizunova and O. Gamayun, arXiv:2010.03385 (2020).
[5] H. Sakaguchi and M. Tamura, J. Phys. Soc. Jpn. **74**, 292 (2005).
[6] C. Weiss and Y. Castin, Phys. Rev. Lett. **102**, 010403 (2009).
[7] A. I. Streltsov, O. E. Alon, and L. S. Cederbaum, Phys. Rev. A **80**, 043616 (2009).
[8] S. D. Hansen, N. Nygaard, and K. Mølmer, Appl. Sci. **11**, 2294 (2021).
[9] O. V. Marchukov, B. A. Malomed, V. A. Yurovsky, M. Olshanii, V. Dunjko, and R. G. Hulet, Phys. Rev. A **99**, 063623 (2019).
[10] V. Dunjko and M. Olshanii, arXiv:1501.00075 (2020).
[11] J. Cuevas, P. G. Kevrekidis, B. A. Malomed, P. Dyke, and R. G. Hulet, New J. Phys. **15**, 063006 (2013).
[12] A. E. Miroshnichenko, S. Flach, and B. Malomed, Chaos **13**, 874 (2003).
[13] K. T. Stoychev and M. T. Primatarowa, and R. S. Kamburova, Phys. Rev. E **70**, 066622 (2004).
[14] C. Lee and J. Brand, Europhys. Lett. **73**, 321 (2006).
[15] T. Ernst and J. Brand, Phys. Rev. A **81**, 033614 (2010).
[16] K. Forinash, M. Peyrard, and B. Malomed, Phys. Rev. E **49**, 3400 (1994).
[17] X. Cao and B. Malomed, Phys. Lett. A **206**, 177 (1995).

[18] D. J. Frantzeskakis, G. Theocharis, F. K. Diakonos, P. Schmelcher, and Y. S. Kivshar, Phys. Rev. A **66**, 053608 (2002).
[19] R. H. Goodman, P. J. Holmes, and M. I. Weinstein, Physica D **192**, 215 (2004).
[20] V. A. Brazhnyi and M. Salerno, Phys. Rev. A **83**, 053616 (2011).
[21] M. O. D. Alotaibi and L. D. Carr, J. Phys. B: Mol. Opt. Phys. **52**, 165301 (2019).
[22] M. Asad-uz-zaman and U. Al Khawaja, Europhys. Lett. **101**, 50008 (2013).
[23] U. Al Khawaja, S. M. Al-Marzoug, H. Bahlouli, and Y. S. Kivshar, Phys. Rev. A **88**, 023830 (2013).
[24] U. Al Khawaja and Andery A. Sukhorukov, Opt. Lett. **40**, 2719 (2015).
[25] I. Kay and H. M. Moses, J. Appl. Phys. **27**, 1503 (1956).
[26] J. Lekner, Am. J. Phys. **875**, 1151 (2007).
[27] U. Al Khawaja and L. Al Sakkaf, *Handbook of Exact Solutions to the Nonlinear Schrödinger Equations* (IOP Publishing, London, 2020).
[28] U. Al Khawaja and Q. M. Al-Mdallal, Int. J. Dif. Eq. **2018**, 6043936 (2018); L. Y. Al Sakkaf, Q. M. Al-Mdallal, and U. Al Khawaja, Complexity **2018**, 8269541 (2018).
[29] G. C. Katsimiga, F. K. Diakonos, and X. N. Maintas, Phys. Lett. B **748**, 117 (2015).